Supplementary Information for *Mechanical relaxation: soft modes of the joint cell–atom Hessian connect crystal structure prediction with the unstable lattices of CALPHAD*

P. Prysiazhniuk, T. A. Shihab, A. Zakrjevsky and G. A. Chass

28 October 2026

All numbers are generated from the data files that accompany the submission (`figures/*/data`) by `build_SI_scirep.py` (derived from `build_SI.py`). Energies in kJ/mol per atom above the SGTE reference structure; $\tau = 0.05\,\mathrm{eV\,\AA^{-2}}$ unless stated otherwise. Sections S3 and S9 are text only.

S1. Targeted set of starting space groups

The targeted set includes, for every element, the space group of the SGTE reference and of known polymorphs (648 generated starts; 22 discarded by the collapse filter described in the Methods). Counts as in Table 1 of the main text.

Element	Starts	Collapsed	Saddle	Hits (BFGS)	Hits (mechanical)	Other minima	Unresolved
As	33	3	26	0	8	25	0
Bi	35	1	33	0	11	24	0
Ce	51	0	38	6	10	41	0
Ga	60	0	45	0	0	60	0
Ge	83	7	53	5	11	70	2
Pt	51	0	34	7	10	38	3
Sb	46	5	42	0	17	29	0
Si	82	5	54	5	10	71	1
Sn	69	0	50	2	4	63	2
Ti	71	1	60	3	27	39	5
U	45	0	31	0	2	41	2
Total	626	22	466	28	110	501	15

Table S1: Targeted-set statistics (GRACE-2L-OMAT).

S2. Sensitivity to the cell weight μ

The same blind starts (random state $1000g + 10N + i$) were rerun with $\mu = N/4$ (Ti, Si; space groups 14, 62, 139) and $\mu = 4N$ (Ti, Si, Sb, Bi; same groups).

μ	Starts	Hits	Hits at $\mu = N$	Same end point	Median c_w of first push (μ / N)
$N/4$	54	8	14	32	0.43 / 0.00
$4N$	108	32	34	78	0.00 / 0.00

Table S2: Hits and end points for the same starts at three cell weights. With $\mu = N/4$ the first push is strain-dominated and seven Ti starts that reach hcp at $\mu = N$ end in fcc.

S3. Determinism and interpolation self-test

Six element–space-group pairs of the blind set (36 starts, $N = 4$ and 8) were rerun on different nodes of the cluster: all end energies, space groups and pushes agree bitwise with the original runs. The minimum-image Fourier interpolation of the force constants was tested on the EMT potential for bcc Cu ($a = 2.88$ Å): eigenvalues of $D(\mathbf{q})$ interpolated from $6 \times 6 \times 6$ force constants at 300 wave vectors commensurate with a $12 \times 12 \times 12$ grid agree with the exact $12 \times 12 \times 12$ values to 5×10^{-6} eV Å^{-2} (median 1×10^{-6}); at 200 random wave vectors $\|D - D^{\dagger}\|/\|D\|$ is 2×10^{-7} with the convention and 0.75 without it; $f_{\mathrm{BZ}}(\tau = 0.05)$ on 5000 random wave vectors is 0.0314 for both grids with the convention and 0.0032 for the $6 \times 6 \times 6$ grid without it.

S4. Sensitivity of the unstable zone fraction to the threshold and the supercell

f_{BZ} from $6 \times 6 \times 6$ force constants (GRACE-2L-OMAT, 20 000 random wave vectors) at six thresholds τ (eV Å^{-2}), and from $4 \times 4 \times 4$ force constants at $\tau = 0.05$; f_{modes} at $\tau = 0.05$. Sixty-one metallic lattices; the regime counts of the main text are unchanged for every τ.

Lattice	0.001	0.01	0.02	0.05	0.1	0.2	4^3, 0.05	f_{modes}
Ag bcc	0.057	0.054	0.050	0.040	0.025	0.004	0.040	0.013
Ag hcp	0.000	0.000	0.000	0.000	0.000	0.000	0.000	0.000
Al bcc	0.354	0.349	0.343	0.327	0.301	0.247	0.335	0.109
Au bcc	0.046	0.042	0.038	0.027	0.012	0.000	0.028	0.009
Be bcc	0.024	0.024	0.023	0.021	0.017	0.011	0.021	0.007
Ce bcc	1.000	1.000	1.000	1.000	0.999	0.996	1.000	0.836
Ce hcp	0.045	0.044	0.043	0.038	0.032	0.020	0.036	0.006
Co bcc	0.090	0.089	0.087	0.081	0.073	0.059	0.075	0.027
Cr fcc	0.463	0.462	0.460	0.454	0.443	0.425	0.445	0.180
Cr hcp	0.492	0.491	0.489	0.484	0.477	0.462	0.474	0.152
Cu bcc	0.040	0.038	0.036	0.029	0.018	0.003	0.030	0.010
Cu hcp	0.000	0.000	0.000	0.000	0.000	0.000	0.000	0.000
Dy bcc	0.656	0.652	0.648	0.635	0.612	0.561	0.634	0.212
Er bcc	0.579	0.574	0.567	0.547	0.510	0.432	0.553	0.182
Ga bcc	0.192	0.171	0.149	0.101	0.045	0.000	0.151	0.034
Ga hcp	0.046	0.031	0.018	0.003	0.000	0.000	0.003	0.001
Gd bcc	0.622	0.617	0.611	0.588	0.550	0.458	0.599	0.196
Hf bcc	0.741	0.740	0.739	0.735	0.728	0.715	0.696	0.253
Hf fcc	0.000	0.000	0.000	0.000	0.000	0.000	0.000	0.000
Ho bcc	0.610	0.605	0.599	0.581	0.552	0.484	0.588	0.194
In bcc	0.098	0.083	0.068	0.032	0.000	0.000	0.044	0.011
Ir bcc	0.954	0.953	0.952	0.951	0.948	0.942	0.902	0.330
Ir hcp	0.000	0.000	0.000	0.000	0.000	0.000	0.000	0.000
La bcc	0.672	0.669	0.666	0.652	0.628	0.580	0.601	0.240
Mg bcc	0.024	0.020	0.016	0.007	0.000	0.000	0.008	0.003
Mo fcc	0.423	0.421	0.420	0.415	0.407	0.389	0.404	0.165
Mo hcp	0.428	0.428	0.427	0.424	0.419	0.409	0.421	0.143
Nb fcc	0.479	0.478	0.476	0.472	0.463	0.445	0.455	0.203

Lattice	0.001	0.01	0.02	0.05	0.1	0.2	4^3, 0.05	f_{modes}
Nb hcp	0.372	0.371	0.370	0.366	0.359	0.345	0.370	0.109
Nd bcc	0.772	0.770	0.767	0.758	0.743	0.711	0.739	0.256
Ni bcc	0.159	0.158	0.155	0.149	0.139	0.122	0.155	0.050
Os bcc	0.920	0.920	0.920	0.919	0.917	0.915	0.927	0.330
Os fcc	0.000	0.000	0.000	0.000	0.000	0.000	0.000	0.000
Pb bcc	0.211	0.199	0.186	0.155	0.112	0.047	0.135	0.052
Pd bcc	0.053	0.050	0.047	0.040	0.029	0.014	0.044	0.013
Pt bcc	0.203	0.202	0.200	0.193	0.182	0.161	0.258	0.064
Pt hcp	0.004	0.004	0.003	0.002	0.000	0.000	0.002	0.000
Re bcc	0.822	0.821	0.820	0.817	0.812	0.802	0.813	0.278
Re fcc	0.000	0.000	0.000	0.000	0.000	0.000	0.000	0.000
Rh bcc	0.724	0.723	0.723	0.720	0.717	0.708	0.746	0.240
Ru bcc	0.895	0.895	0.895	0.893	0.891	0.888	0.896	0.314
Ru fcc	0.000	0.000	0.000	0.000	0.000	0.000	0.000	0.000
Sc bcc	0.187	0.183	0.178	0.166	0.145	0.109	0.169	0.055
Ta fcc	0.435	0.433	0.432	0.427	0.420	0.407	0.422	0.171
Ta hcp	0.369	0.367	0.366	0.361	0.353	0.334	0.355	0.103
Tb bcc	0.696	0.692	0.689	0.676	0.655	0.609	0.677	0.225
Tc bcc	0.895	0.894	0.892	0.889	0.883	0.870	0.878	0.313
Th bcc	0.628	0.626	0.624	0.618	0.606	0.582	0.603	0.209
Ti bcc	0.652	0.650	0.648	0.640	0.627	0.604	0.592	0.216
Ti fcc	0.000	0.000	0.000	0.000	0.000	0.000	0.000	0.000
Ti hcp	0.000	0.000	0.000	0.000	0.000	0.000	0.000	0.000
V fcc	0.454	0.453	0.451	0.446	0.436	0.419	0.443	0.168
V hcp	0.454	0.452	0.450	0.445	0.436	0.419	0.437	0.130
W bcc	0.000	0.000	0.000	0.000	0.000	0.000	0.000	0.000
W fcc	0.309	0.308	0.306	0.303	0.296	0.285	0.301	0.116
W hcp	0.325	0.325	0.324	0.322	0.318	0.309	0.317	0.111
Y bcc	0.576	0.569	0.561	0.540	0.500	0.415	0.546	0.180
Yb bcc	0.118	0.114	0.111	0.098	0.082	0.055	0.108	0.033
Zn bcc	0.427	0.423	0.418	0.401	0.374	0.315	0.397	0.134
Zr bcc	0.665	0.662	0.660	0.652	0.640	0.617	0.616	0.219
Zr fcc	0.000	0.000	0.000	0.000	0.000	0.000	0.000	0.000

Table S3: Unstable zone fraction against threshold and supercell.

S5. Provenance of the SGTE lattice stabilities

Intercept a and slope b of the linear fit $\Delta G = a + bT$ (300–3000 K) to the SGTE unary database, relative to the reference structure (for Zn the SER phase HCP_ZN); static energy with its source; provenance class as used in the main text (sources after Dinsdale 1991).

Lattice	Ref.	a (kJ/mol)	b (J/mol/K)	E_0 (kJ/mol)	Source	Provenance
Ag bcc	fcc	3.4	−1.05	2.3	DFT	extrap., Saunders 1988
Al bcc	fcc	10.1	−4.81	9.5	DFT	extrap., Kaufman–Bernstein 1970
As bcc	RHOMBOHEDRAL A7	24.9	−16.10	44.5	GRACE	p-block (estimate rule)
As fcc	RHOMBOHEDRAL A7	24.9	−14.74	53.2	GRACE	p-block (estimate rule)
As hcp	RHOMBOHEDRAL A7	24.9	−14.00	49.7	GRACE	p-block (estimate rule)
Au bcc	fcc	4.2	−1.10	1.7	DFT	extrap., Saunders 1988
Be bcc	hcp	6.4	−4.04	9.6	DFT	real allotrope (fitted)
Bi bcc	RHOMBOHEDRAL A7	11.3	−13.90	12.1	GRACE	p-block (estimate rule)
Bi bct	RHOMBOHEDRAL A7	4.2	–	4.5	GRACE	p-block (estimate rule)
Bi fcc	RHOMBOHEDRAL A7	9.9	−12.50	12.4	GRACE	p-block (estimate rule)
Bi hcp	RHOMBOHEDRAL A7	9.9	−11.80	11.6	GRACE	p-block (estimate rule)
C diamond	GRAPHITE	1.3	4.70	14.1	GRACE	p-block (estimate rule)

Lattice	Ref.	a (kJ/mol)	b (J/mol/K)	E_0 (kJ/mol)	Source	Provenance
Ce bcc	fcc	2.3	−2.38	21.6	DFT	real allotrope (fitted)
Ce hcp	fcc	0.3	0.00	8.7	DFT	f-block
Co bcc	hcp	2.9	−0.71	8.1	GRACE	extrap., KTH 1987–88
Cr fcc	bcc	7.3	0.16	36.0	GRACE	extrap., KTH 1987–88
Cr hcp	bcc	4.4	0.00	34.4	GRACE	extrap., KTH 1987–88
Cu bcc	fcc	4.0	−1.26	3.7	DFT	extrap., Saunders 1988
Dy bcc	hcp	2.6	−1.89	13.0	DFT	f-block
Er bcc	hcp	4.6	−2.49	13.6	DFT	f-block
Ga bcc	ORTHORHOMBIC GA	4.5	−11.70	2.0	GRACE	p-block (estimate rule)
Ga hcp	ORTHORHOMBIC GA	4.5	−9.50	1.4	GRACE	p-block (estimate rule)
Gd bcc	hcp	2.9	−1.83	12.3	DFT	f-block
Ge bcc	DIAMOND A4	34.1	−23.50	32.5	GRACE	p-block (estimate rule)
Ge fcc	DIAMOND A4	36.0	−22.30	32.4	GRACE	p-block (estimate rule)
Ge hcp	DIAMOND A4	35.0	−21.50	33.3	GRACE	p-block (estimate rule)
Hf bcc	hcp	9.4	−4.28	17.3	DFT	real allotrope (fitted)
Ho bcc	hcp	3.3	−1.56	13.3	DFT	f-block
In bcc	TETRAGONAL A6	0.8	−0.80	1.6	GRACE	p-block (estimate rule)
Ir bcc	fcc	32.0	−6.90	58.6	DFT	extrap., Saunders 1988
La bcc	DHCP	4.9	−5.46	11.8	DFT	f-block
Mg bcc	hcp	3.1	−2.10	2.6	DFT	extrap., Saunders 1988
Mo fcc	bcc	15.2	0.63	40.7	DFT	extrap., KTH 1987–88
Mo hcp	bcc	11.6	0.00	41.2	DFT	extrap., KTH 1987–88
Nb fcc	bcc	13.5	1.70	30.1	DFT	extrap., KTH 1987–88
Nb hcp	bcc	10.0	2.40	27.4	DFT	extrap., KTH 1987–88
Nd bcc	DHCP	1.2	−0.98	11.5	DFT	f-block
Ni bcc	fcc	8.7	−3.56	9.0	GRACE	extrap., Dinsdale unpubl.
Os bcc	hcp	27.5	−4.40	85.1	DFT	extrap., Saunders 1988
Pb bcc	fcc	2.4	−1.10	3.4	DFT	p-block (estimate rule)
Pd bcc	fcc	10.5	−1.80	4.3	DFT	extrap., Saunders 1988
Pt bcc	fcc	15.0	−2.40	10.1	DFT	extrap., Saunders 1988
Pt hcp	fcc	2.5	0.10	5.3	DFT	extrap., Saunders 1988
Re bcc	hcp	17.0	−3.70	30.7	DFT	extrap., Dinsdale unpubl.
Rh bcc	fcc	19.0	−4.70	33.2	DFT	extrap., Saunders 1988
Ru bcc	hcp	21.5	−5.05	58.4	GRACE	extrap., Dinsdale unpubl.
Sb bcc	RHOMBOHEDRAL A7	19.9	−15.10	23.1	GRACE	p-block (estimate rule)
Sb bct	RHOMBOHEDRAL A7	13.0	–	11.4	GRACE	p-block (estimate rule)
Sb fcc	RHOMBOHEDRAL A7	19.9	−13.70	28.5	GRACE	p-block (estimate rule)
Sb hcp	RHOMBOHEDRAL A7	19.9	−13.00	25.6	GRACE	p-block (estimate rule)
Sc bcc	hcp	3.0	−2.12	10.0	DFT	real allotrope (fitted)
Si bcc	DIAMOND A4	47.0	−22.50	49.8	GRACE	p-block (estimate rule)
Si fcc	DIAMOND A4	51.0	−21.80	52.0	GRACE	p-block (estimate rule)
Si hcp	DIAMOND A4	49.2	−20.80	50.5	GRACE	p-block (estimate rule)
Sn bcc	BCT A5	4.4	−6.00	2.3	GRACE	p-block (estimate rule)
Sn diamond	BCT A5	−2.6	8.37	0.0	GRACE	p-block (estimate rule)
Sn fcc	BCT A5	5.5	−8.46	1.4	GRACE	p-block (estimate rule)
Sn hcp	BCT A5	3.9	−7.65	1.9	GRACE	p-block (estimate rule)
Ta fcc	bcc	16.0	1.70	22.8	DFT	extrap., KTH 1987–88
Ta hcp	bcc	12.0	2.40	26.5	DFT	extrap., KTH 1987–88
Tb bcc	hcp	3.8	−2.31	12.6	DFT	f-block
Tc bcc	hcp	18.0	−4.50	23.9	DFT	extrap., Saunders 1988
Th bcc	fcc	4.6	−2.32	11.9	DFT	real allotrope (fitted)
Ti bcc	hcp	3.2	−2.04	10.6	DFT	real allotrope (fitted)
V fcc	bcc	7.5	1.70	22.8	DFT	extrap., KTH 1987–88
V hcp	bcc	4.0	2.40	23.9	DFT	extrap., KTH 1987–88
W fcc	bcc	19.3	0.63	43.1	GRACE	extrap., KTH 1987–88
W hcp	bcc	14.8	0.00	45.7	GRACE	extrap., KTH 1987–88
Y bcc	hcp	5.8	−3.00	11.9	DFT	real allotrope (fitted)

Lattice	Ref.	a (kJ/mol)	b (J/mol/K)	E_0 (kJ/mol)	Source	Provenance
Yb bcc	fcc	2.0	−2.33	16.9	DFT	real allotrope (fitted)
Zn bcc	hcp	2.9	−2.51	8.3	DFT	extrap., Kaufman 1970
Zr bcc	hcp	2.7	−1.52	8.0	DFT	real allotrope (fitted)

Table S4: SGTE values and their provenance.

S6. Born level against inflection detection, phase by phase

Extrapolated phases for which both the Born level E_B (Methods, DFT scale, softest-mode path) and the inflection-detection value of Chen et al. (2025) exist. Deviations from the SGTE intercept a. bcc Co is listed for completeness but excluded from the statistics: Chen et al. refer it to fcc Co, whereas the SGTE intercept and our level refer to hcp Co. RMS over the 17 phases: E_B 4.57, inflection detection 6.59, $0.38\,E_0$ 5.04 kJ/mol; mean absolute errors 3.51 and 5.40; E_B is closer in 11 of 17. Removing all phases of any one element leaves the RMS of E_B between 3.7 (Nb removed) and 4.9 and that of inflection detection between 5.9 and 6.9.

Lattice	E_0	SGTE a	E_B	Chen 2025	$0.38\,E_0$	$E_B - a$	Chen$-a$
Co bcc*	8.1	2.9	4.3	3.3	3.1	+1.4	+0.4
Ni bcc	9.0	8.7	4.2	9.1	3.4	−4.6	+0.4
Al bcc	9.5	10.1	4.4	4.4	3.6	−5.6	−5.7
V fcc	22.8	7.5	3.4	4.4	8.7	−4.1	−3.1
Ta fcc	22.8	16.0	15.0	16.2	8.7	−1.0	+0.2
Tc bcc	23.9	18.0	16.5	4.4	9.1	−1.5	−13.6
Ta hcp	26.5	12.0	12.8	8.1	10.1	+0.8	−3.9
Nb hcp	27.4	10.0	11.7	6.5	10.4	+1.7	−3.5
Nb fcc	30.1	13.5	1.4	19.4	11.4	−12.1	+5.9
Re bcc	30.7	17.0	19.0	15.2	11.7	+2.0	−1.8
Rh bcc	33.2	19.0	18.0	15.6	12.6	−1.0	−3.4
Mo fcc	40.7	15.2	19.0	22.5	15.5	+3.8	+7.3
Mo hcp	41.2	11.6	14.3	23.4	15.6	+2.7	+11.8
W fcc	43.1	19.3	21.1	25.9	16.4	+1.8	+6.6
W hcp	45.7	14.8	16.3	17.9	17.4	+1.5	+3.1
Ru bcc	58.4	21.5	25.9	16.8	22.2	+4.4	−4.7
Ir bcc	58.6	32.0	29.5	43.9	22.3	−2.5	+11.9
Os bcc	85.1	27.5	36.2	22.6	32.3	+8.7	−4.9

Table S5: Levels against SGTE on the common phases (kJ/mol). *bcc Co: different reference phase in Chen et al. (fcc) and here (hcp); not included in the statistics.

S7. The two regimes on 53 phases

The 29 extrapolated phases with a descent path (main text) and 24 further metallic phases with an SGTE value but no path (mostly mechanically stable fcc and hcp forms of hcp and fcc metals), ordered by $x = E_0/(k_B T_m)$ with T_m the melting point of the reference phase from the SGTE liquid. Static energies from DFT where available, otherwise from GRACE-2L-OMAT, always relative to the SGTE reference phase of the element. Below $x = 0.8$ (33 phases) $|a - E_0| \leq 3$ kJ/mol in 24 and ≤ 6 in 31 (median 1.4; outside: bcc Pd +6.2, hcp Fe −10.6); above (20 phases) the median of $a - E_0$ is −18.6 kJ/mol, or $-0.63\,E_0$.

Lattice	E_0 (kJ/mol)	a (kJ/mol)	a/E_0	x	Set
Sr hcp	0.3	0.2	0.87	0.03	no path, DFT
Ca hcp	0.3	0.5	1.45	0.04	no path, DFT

Lattice	E_0 (kJ/mol)	a (kJ/mol)	a/E_0	x	Set
Au hcp	1.0	0.2	0.25	0.09	no path, DFT
Cu hcp	1.0	0.6	0.58	0.09	no path, GRACE
Ti fcc	1.9	6.0	3.14	0.13	no path, GRACE
Ni hcp	1.9	1.0	0.54	0.13	no path, GRACE
Mg fcc	1.1	2.6	2.35	0.14	no path, DFT
Au bcc	1.7	4.2	2.53	0.15	path
Ba hcp	1.3	2.0	1.52	0.16	no path, DFT
Y fcc	2.5	6.0	2.43	0.17	no path, DFT
Rh hcp	3.3	3.0	0.90	0.18	no path, GRACE
Zr fcc	3.3	7.6	2.31	0.20	no path, GRACE
Ba fcc	1.7	1.8	1.08	0.20	no path, DFT
Pd hcp	3.0	2.0	0.66	0.20	no path, DFT
Re fcc	6.0	11.0	1.83	0.21	no path, GRACE
Ag bcc	2.3	3.4	1.45	0.23	path
Ir hcp	5.6	4.0	0.71	0.25	no path, GRACE
Pd bcc	4.3	10.5	2.45	0.28	path
Sc fcc	4.2	5.0	1.20	0.28	no path, GRACE
Tc fcc	6.2	10.0	1.62	0.31	no path, GRACE
Pt hcp	5.3	2.5	0.47	0.31	path
Cu bcc	3.7	4.0	1.08	0.33	path
Mg bcc	2.6	3.1	1.19	0.34	path
Hf fcc	7.1	10.0	1.41	0.35	no path, DFT
Al hcp	3.2	5.5	1.69	0.42	no path, GRACE
Ru fcc	10.3	12.5	1.22	0.47	no path, GRACE
Fe hcp	7.1	−3.4	−0.48	0.48	no path, DFT
Os fcc	13.3	13.0	0.98	0.48	no path, GRACE
Zn fcc	3.2	3.0	0.93	0.56	no path, DFT
Co bcc	8.1	2.9	0.36	0.58	path
Pt bcc	10.1	15.0	1.49	0.59	path
Be fcc	7.8	6.3	0.82	0.61	no path, DFT
Ni bcc	9.0	8.7	0.97	0.63	path
Ta fcc	22.8	16.0	0.70	0.83	path
Ta hcp	26.5	12.0	0.45	0.97	path
Re bcc	30.7	17.0	0.55	1.07	path
Tc bcc	23.9	18.0	0.75	1.19	path
Nb hcp	27.4	10.0	0.36	1.20	path
Al bcc	9.5	10.1	1.06	1.22	path
V fcc	22.8	7.5	0.33	1.26	path
V hcp	23.9	4.0	0.17	1.32	path
Nb fcc	30.1	13.5	0.45	1.32	path
W fcc	43.1	19.3	0.45	1.40	path
Zn bcc	8.3	2.9	0.35	1.44	path
W hcp	45.7	14.8	0.32	1.49	path
Mo fcc	40.7	15.2	0.37	1.69	path
Mo hcp	41.2	11.6	0.28	1.71	path
Rh bcc	33.2	19.0	0.57	1.79	path
Cr hcp	34.4	4.4	0.13	1.90	path
Cr fcc	36.0	7.3	0.20	1.99	path
Ir bcc	58.6	32.0	0.55	2.59	path
Ru bcc	58.4	21.5	0.37	2.70	path
Os bcc	85.1	27.5	0.32	3.10	path

Table S6: Extrapolated SGTE values against the static energy and the thermal energy at the melting point of the reference.

S8. Harmonic estimate from the stable branches

$\Delta S_{\mathrm{harm}} = -3R\,(\langle \ln \omega \rangle_{\mathrm{lattice}} - \langle \ln \omega \rangle_{\mathrm{ref}})$ over the stable $(\mathbf{q}, b)$ pairs of $6 \times 6 \times 6$ force constants (Methods); fraction of modes used f_{used} (modes with $\lambda > \tau$; it differs from $1 - f_{\mathrm{modes}}$ by the modes within $\pm\tau$ of

zero, typically about 1 % (median 1.0 %, up to 6.8 % for bcc Ga), and the same definition is used in Section S14). The estimate is reported for lattices with $f_{\mathrm{used}} \geq 0.75$ (adopted applicability criterion); the excluded lattices (bcc Ce, Hf, Ir, La, Nd, Os, Re, Ru, Tc) are listed for completeness and marked. Reference entropy (unstable phase minus reference phase): $-b$ of the SGTE fit over 300–3000 K for extrapolated and estimated phases; the entropy of the measured transition, $-\mathrm{d}\Delta G/\mathrm{d}T$ at the transition temperature of the SGTE description, for real allotropes; the inflection-detection value of Chen et al. (2025) where available. hcp Ce carries an SGTE slope of zero by convention. $\mathrm{J\,mol^{-1}\,K^{-1}}$.

Lattice	Class	f_{BZ}	f_{used}	ΔS_{harm}	Ref.	Type of reference	Chen 2025
Ni bcc	extrap., Dinsdale unpubl.	0.149	0.943	+3.44	+3.56	SGTE slope 300–3000 K	+1.26
Re bcc†	extrap., Dinsdale unpubl.	0.817	0.718	+5.52	+3.70	SGTE slope 300–3000 K	+4.10
Ru bcc†	extrap., Dinsdale unpubl.	0.893	0.683	+13.76	+5.05	SGTE slope 300–3000 K	+4.10
Co bcc	extrap., KTH 1987–88	0.081	0.966	+4.69	+0.71	SGTE slope 300–3000 K	–
W fcc	extrap., KTH 1987–88	0.303	0.877	+9.79	−0.63	SGTE slope 300–3000 K	+6.00
W hcp	extrap., KTH 1987–88	0.322	0.884	+9.06	0.00	SGTE slope 300–3000 K	+3.30
Ta hcp	extrap., KTH 1987–88	0.361	0.889	+5.68	−2.40	SGTE slope 300–3000 K	−0.04
Nb hcp	extrap., KTH 1987–88	0.366	0.880	+3.81	−2.40	SGTE slope 300–3000 K	−1.13
Mo fcc	extrap., KTH 1987–88	0.415	0.827	+10.06	−0.63	SGTE slope 300–3000 K	+4.07
Mo hcp	extrap., KTH 1987–88	0.424	0.850	+8.23	0.00	SGTE slope 300–3000 K	+2.81
Ta fcc	extrap., KTH 1987–88	0.427	0.818	+4.79	−1.70	SGTE slope 300–3000 K	+1.69
V hcp	extrap., KTH 1987–88	0.445	0.860	+1.76	−2.40	SGTE slope 300–3000 K	−0.39
V fcc	extrap., KTH 1987–88	0.446	0.821	+0.36	−1.70	SGTE slope 300–3000 K	−1.63
Cr fcc	extrap., KTH 1987–88	0.454	0.810	+10.39	−0.16	SGTE slope 300–3000 K	–
Nb fcc	extrap., KTH 1987–88	0.472	0.788	+3.94	−1.70	SGTE slope 300–3000 K	−0.58
Cr hcp	extrap., KTH 1987–88	0.484	0.840	+9.66	0.00	SGTE slope 300–3000 K	–
Zn bcc	extrap., Kaufman 1970	0.401	0.848	+0.94	+2.51	SGTE slope 300–3000 K	–
Al bcc	extrap., Kaufman–Bernstein	0.327	0.874	+2.03	+4.81	SGTE slope 300–3000 K	+3.47
Pt hcp	extrap., Saunders 1988	0.002	0.998	+2.15	−0.10	SGTE slope 300–3000 K	–
Mg bcc	extrap., Saunders 1988	0.007	0.980	+1.84	+2.10	SGTE slope 300–3000 K	–
Au bcc	extrap., Saunders 1988	0.027	0.977	+0.60	+1.10	SGTE slope 300–3000 K	–
Cu bcc	extrap., Saunders 1988	0.029	0.982	+2.15	+1.26	SGTE slope 300–3000 K	–
Pd bcc	extrap., Saunders 1988	0.040	0.977	+2.57	+1.80	SGTE slope 300–3000 K	–
Ag bcc	extrap., Saunders 1988	0.040	0.973	+1.81	+1.05	SGTE slope 300–3000 K	–
Pt bcc	extrap., Saunders 1988	0.193	0.929	+2.57	+2.40	SGTE slope 300–3000 K	+2.04
Rh bcc	extrap., Saunders 1988	0.720	0.756	+5.53	+4.70	SGTE slope 300–3000 K	+4.57
Tc bcc†	extrap., Saunders 1988	0.889	0.682	+5.52	+4.50	SGTE slope 300–3000 K	+0.16
Os bcc†	extrap., Saunders 1988	0.919	0.667	+14.68	+4.40	SGTE slope 300–3000 K	+3.02
Ir bcc†	extrap., Saunders 1988	0.951	0.667	+9.67	+6.90	SGTE slope 300–3000 K	+5.77
Ce hcp	f-block	0.038	0.990	+7.57	0.00	SGTE slope 300–3000 K	–
Er bcc	f-block	0.547	0.797	+3.95	+2.49	transition, 1844 K	–
Ho bcc	f-block	0.581	0.788	+3.29	+2.33	transition, 1758 K	–
Gd bcc	f-block	0.588	0.783	+3.84	+2.42	transition, 1508 K	–
Dy bcc	f-block	0.635	0.775	+3.09	+2.77	transition, 1654 K	–
La bcc†	f-block	0.652	0.735	+5.54	+3.27	transition, 992 K	–
Tb bcc	f-block	0.676	0.762	+2.62	+2.80	transition, 1562 K	–
Nd bcc†	f-block	0.758	0.731	+4.71	+2.68	transition, 1128 K	–
Ga hcp	p-block	0.003	0.970	+10.04	+9.50	SGTE slope 300–3000 K	–
In bcc	p-block	0.032	0.935	+1.14	+0.80	SGTE slope 300–3000 K	–
Ga bcc	p-block	0.101	0.899	+8.17	+11.70	SGTE slope 300–3000 K	–
Pb bcc	p-block	0.155	0.909	+2.00	+1.10	SGTE slope 300–3000 K	+2.84
Be bcc	real allotrope	0.021	0.990	+3.06	+4.49	transition, 1527 K	–
Yb bcc	real allotrope	0.098	0.950	+3.07	+1.68	transition, 1033 K	–
Sc bcc	real allotrope	0.166	0.927	+5.80	+2.49	transition, 1608 K	+3.33
Y bcc	real allotrope	0.540	0.797	+3.13	+2.79	transition, 1751 K	–
Th bcc	real allotrope	0.618	0.781	+8.56	+2.20	transition, 1633 K	–
Ti bcc	real allotrope	0.640	0.774	+3.97	+3.60	transition, 1155 K	–

Lattice	Class	f_{BZ}	f_{used}	ΔS_{harm}	Ref.	Type of reference	Chen 2025
Zr bcc	real allotrope	0.652	0.771	+3.05	+3.59	transition, 1139 K	–
Hf bcc†	real allotrope	0.735	0.741	+3.35	+2.90	transition, 2016 K	–
Ce bcc†	real allotrope	1.000	0.142	+28.98	+2.99	transition, 1000 K	–

Table S7: Entropy estimate from the stable branches against reference values. † $f_{\mathrm{used}} < 0.75$: excluded from the statistics of the main text.

S9. Structural verification of hits and hubs

Hits: each end structure of the 222 candidate hits of the blind set (space group of the reference, energy within 0.5 kJ/mol) was compared with the reference built from its prototype using spglib (tolerance 0.05 Å): space group, number of atoms in the primitive cell and the sizes of the orbits of equivalent atoms. 221 agree; the exception is the Ga start in space group 14 with $N = 12$, which ends in a *Cmce* structure with six atoms in the primitive cell and two orbits, 0.44 kJ/mol above α-Ga (one orbit, four atoms). It is counted as a miss in Table 1 of the main text and in the comparison of schemes (Section S18), also for ordinary relaxation. Hubs: the saddle frames of the 96 trajectories that pass through the hubs of Fig. 4 of the main text were analysed in the same way: all 78 visits to the simple-cubic hubs of As (12), Sb (24), Bi (13) and Si (12) and to the bct (10) and bcc (7) hubs of Ti are the one-atom lattices; of the seven saddle visits to the simple-hexagonal nodes of Si and Ge, four are the one-atom lattice and three are a two-atom $P6/mmm$ structure (Wyckoff 2*c*; an AA-stacked honeycomb with $a = 4.43$, $c = 2.79$ Å for Ge) that the potential puts within 0.05 kJ/mol of the simple-hexagonal lattice and that spglib does not reduce at tolerances up to 0.3 Å. Among the end points of the blind set, 38 Si and 3 Ge trajectories end in the one-atom simple-hexagonal lattice and 1 Ge trajectory in the honeycomb. Canonicalisation: spglib standardisation to the primitive cell (tolerance 0.05 Å); node identity in the network uses the space group and the energy (0.5 kJ/mol bins). Representative POSCAR files of every hub (simple cubic As, Sb, Bi, Si; simple hexagonal Ge; the honeycomb nodes of Ge and Si; bct and bcc Ti) accompany the submission (`SI_structure_check/data/hub_structures`, with a README listing the source trajectory of each).

S10. DFT force constants of $4 \times 4 \times 4$ supercells

	f_{BZ}		f_{modes}		λ_{min} (eV Å^{-2})		imaginary modes on the grid	
Lattice	DFT	GRACE	DFT	GRACE	DFT	GRACE	DFT	GRACE
Cu bcc	0.032	0.030	0.011	0.010	−0.23	−0.21	18	18
W fcc	0.449	0.301	0.185	0.107	−5.77	−3.14	36	28
Ti bcc	0.601	0.592	0.234	0.200	−4.94	−2.60	48	42

Table S8: DFT (IBRION = 6, 480 eV, k-spacing 0.12 Å^{-1}) against GRACE-2L-OMAT, $4 \times 4 \times 4$ supercells, $\tau = 0.05$; the GRACE values of f_{BZ}, f_{modes} and λ_{min} are for the ideal lattice relaxed with the potential (20 000 wave vectors). For fcc W, 8 of the 36 DFT modes lie within 5 cm^{-1} of zero; the deep DFT modes are at 61–75 cm^{-1} against 38–46 cm^{-1} on the potential. For bcc Ti the deepest DFT modes are at 164 cm^{-1} against 77 cm^{-1}.

S11. Hits within a budget of evaluations

Number of the 884 common blind starts not solved by ordinary relaxation that reach the reference with at most B evaluations of the potential per start (Hessians and candidate scans included; one evaluation = one call returning energy, forces and stress).

Scheme	$B = 1\,000$	$B = 3\,000$	$B = 10\,000$	$B = 30\,000$	$B = 100\,000$
joint cell–atom Hessian	17	70	92	126	126
atomic modes, same scan	16	67	82	110	110
strain modes, same scan	7	17	27	46	46
atomic modes, first protocol	13	45	54	70	94
strain modes, first protocol	2	14	29	39	47
random push, realisation 1	6	9	46	135	183
random push, realisation 2	8	15	49	145	184

Table S9: New hits within a budget per start.

S12. Born level along the path: DFT profiles

For each frame k of the softest-mode descent on the potential, listed in the order of the descent: DFT energy above the relaxed reference, smallest eigenvalue of the DFT joint Hessian λ_{joint} (eV Å^{-2}; assembled by least squares from the forces and stresses of the ± 0.015 Å displacements of every atom and the $\pm 0.5\,\%$ strains of IBRION = 6, ISIF = 3, ISYM = 0, in the generalised coordinates of the Methods with $\mu = N$, symmetrised, translations projected out), the number of imaginary non-translational modes among the phonon frequencies printed by VASP (above 0.3 THz; the translational modes, which VASP prints as imaginary frequencies of 0.30–0.35 THz in some one-atom cells, are excluded), and the frames that bracket E_B (upper and lower). E_B is the last change of sign of λ_{joint} from negative to non-negative along the path, confirmed only if all later frames are stable. Six representative paths are shown; the file `EB_profiles_dft_all_paths.csv` holds all 61 paths: 50 confirmed brackets; bcc In unconfirmed (the instability returns in the last two frames); bcc Yb with a change from stable to unstable only; and 9 paths on which the instability persists below the lowest computed frame, so that no level is assigned. Over the 50 confirmed brackets the width has a median of 0.76 kJ/mol (interquartile range 0.40–1.46, maximum 4.9 for bcc Re). The file `ib6_recheck.csv` lists for each of the 599 frames the number of atoms, the number of $\pm$ pairs, the rank of the perturbation matrix (equal to $3N + 6$ in every frame), the asymmetry removed by the symmetrisation (median 0.03, maximum 0.6 eV Å^{-2}), λ_{joint}, the smallest eigenvalue and the number of negative eigenvalues of the atomic block after projection of the translations, and the imaginary VASP frequencies with their translational character; the sign of the projected atomic block agrees with the VASP count in 435 of the 443 frames with two or more atoms, the exceptions being modes between -0.05 and -0.005 eV Å^{-2}, below the 0.3 THz cutoff. VASP's simple shears include a rotation, and correcting for it shifts E_B by at most 0.4 kJ/mol.

Path	frame k	E_{DFT} (kJ/mol)	λ_{joint}	imag. modes (non-transl.)	bracket
W fcc	5	38.39	−13.672	0	
	8	31.88	−5.278	0	
	9	29.62	−5.413	0	
	11	24.97	−3.166	0	
	12	22.57	−1.008	0	upper
	13	20.14	0.660	0	lower
	14	17.71	2.604	0	
	16	12.98	9.457	0	
	18	8.64	11.389	0	
$E_B = 21.10$ kJ/mol; SGTE 19.3					
Ru bcc	7	53.76	−17.137	1	
	11	48.77	−13.150	1	
	14	44.63	−9.830	0	
	17	40.31	−6.924	0	
	20	35.93	−4.582	0	
	22	33.01	−3.208	0	
	23	31.56	−2.561	0	

Path	frame k	E_{DFT} (kJ/mol)	λ_{joint}	imag. modes (non-transl.)	bracket
	25	28.68	−1.289	0	
	26	27.26	−0.634	0	upper
	27	25.84	0.047	0	lower
	28	24.45	0.755	0	
	29	23.07	1.478	0	
	30	21.71	2.179	0	
	31	20.38	2.829	0	
	32	19.07	3.404	0	
$E_B = 25.94$ kJ/mol; SGTE 21.5					
Nb fcc	2	28.24	−22.433	0	
	5	23.94	−16.141	0	
	6	22.27	−14.467	0	
	7	20.55	−13.172	0	
	8	18.83	−12.273	0	
	10	15.46	−11.336	0	
	12	12.16	−10.601	0	
	15	7.59	−8.899	0	
	17	5.07	−6.947	0	
	21	1.52	−0.251	0	upper
	23	0.52	2.444	0	lower
$E_B = 1.43$ kJ/mol; SGTE 13.5					
Mo hcp	44	15.33	−0.527	0	upper
	46	13.88	0.207	0	lower
	48	12.45	0.669	0	
	50	11.03	1.018	0	
$E_B = 14.29$ kJ/mol; SGTE 11.6					
Rh bcc	5	27.70	−13.879	0	
	7	24.44	−9.070	0	
	9	20.89	−4.140	0	
	10	19.05	−1.625	0	upper
	11	17.29	1.129	0	lower
	12	15.43	3.645	0	
	14	11.84	7.009	0	
	16	8.52	10.537	0	
	18	5.60	10.991	0	
$E_B = 18.01$ kJ/mol; SGTE 19.0					
Al bcc	6	7.76	−5.384	0	
	8	6.74	−2.837	0	
	9	6.44	−6.544	0	
	11	5.18	−1.140	0	upper
	13	3.86	0.912	0	lower
	14	3.30	1.659	0	
	16	2.34	0.920	0	
	18	1.47	1.869	0	
$E_B = 4.45$ kJ/mol; SGTE 10.1					

Table S10: DFT profiles along the softest-mode path for six representative lattices.

S13. Route and cell dependence of the Born level on the potential

For each unstable lattice, all mode-following trajectories on GRACE-2L-OMAT that reach the reference (softest and higher unstable subspaces, both senses, one- and two-atom cells): number of such routes, E_B along the softest route, the lowest and highest E_B over routes and their spread, and the median E_B in the one-atom and in the larger cells. kJ/mol.

Lattice	E_0 (GRACE)	routes	E_B softest	min	max	spread	$N = 1$	$N > 1$
Ag bcc	3.0	2	1.24	1.23	1.24	0.01	1.24	–
Al bcc	9.0	2	4.45	2.86	4.45	1.59	3.65	–
Au bcc	2.2	2	0.56	0.56	0.91	0.35	0.73	–
Be bcc	6.0	4	2.64	2.46	2.65	0.19	–	2.55
Cd bcc	3.9	4	1.14	0.90	1.14	0.24	–	0.90
Ce bcc	21.3	10	3.22	2.31	5.76	3.45	4.17	3.23
Co bcc	8.1	4	3.55	3.29	3.55	0.26	–	3.35
Cr fcc	36.0	9	16.88	5.44	16.88	11.44	14.00	7.00
Cr hcp	34.4	11	12.43	5.77	17.22	11.45	–	12.43
Cu bcc	4.0	2	1.77	1.77	1.77	0.00	1.77	–
Dy bcc	12.2	4	5.77	3.69	5.77	2.08	–	5.05
Er bcc	12.0	4	5.55	3.76	5.55	1.79	–	5.52
Gd bcc	7.9	4	3.53	2.61	3.59	0.98	–	3.56
Hf bcc	15.7	4	5.63	3.11	6.21	3.10	–	5.92
Ho bcc	12.0	4	5.57	3.32	5.57	2.25	–	5.54
In bcc	1.6	6	0.80	0.70	0.80	0.11	0.75	0.73
Ir bcc	56.1	2	22.85	13.92	22.85	8.93	18.39	–
Mg bcc	2.6	4	1.07	1.06	1.07	0.01	–	1.06
Mo fcc	40.4	10	19.90	4.39	19.90	15.51	15.49	7.62
Mo hcp	39.7	11	12.34	5.58	15.55	9.97	–	12.26
Nb fcc	30.1	12	0.50	0.50	12.01	11.51	9.48	4.50
Nb hcp	26.3	13	11.41	3.54	11.77	8.23	–	9.47
Ni bcc	9.0	2	4.37	3.70	4.37	0.66	4.04	–
Os bcc	84.3	6	16.20	11.96	32.79	20.83	–	20.15
Pb bcc	3.9	2	1.92	1.67	1.92	0.25	1.79	–
Pd bcc	4.8	4	2.63	1.11	2.63	1.52	2.23	1.14
Pt bcc	8.4	6	0.57	0.57	0.91	0.34	0.78	0.74
Re bcc	33.1	8	14.31	9.17	14.31	5.15	–	11.40
Rh bcc	30.5	3	15.33	9.22	15.33	6.10	12.28	12.46
Ru bcc	58.4	4	13.10	8.85	23.49	14.64	–	18.29
Sc bcc	7.4	4	3.47	2.99	3.47	0.48	–	3.40
Sm bcc	10.7	2	1.19	1.19	3.50	2.31	–	2.34
Ta fcc	25.6	9	11.20	4.78	11.41	6.63	10.88	8.92
Ta hcp	25.5	9	12.80	7.03	13.74	6.71	–	11.16
Tb bcc	11.7	4	5.60	3.47	5.60	2.13	–	4.61
Tc bcc	25.3	8	9.69	6.32	11.26	4.94	–	9.46
Th bcc	14.2	2	5.83	3.34	5.83	2.49	4.58	–
Ti bcc	7.7	4	2.14	1.79	2.44	0.65	–	2.29
V fcc	22.1	12	0.78	0.54	5.10	4.56	4.41	2.00
V hcp	20.7	11	0.90	0.28	6.37	6.10	–	2.41
W fcc	43.1	10	21.36	4.49	21.36	16.87	18.24	11.91
W hcp	45.7	12	15.16	6.41	19.65	13.24	–	13.41
Y bcc	10.8	4	5.08	3.37	5.20	1.83	–	5.14
Zn bcc	6.2	4	1.94	1.18	2.08	0.90	–	2.01
Zr bcc	8.2	4	3.09	1.72	3.20	1.47	–	3.14

Table S11: Route and cell dependence of E_B on the potential (45 lattices). Median spread 2.3 kJ/mol (interquartile range 0.7–6.7); in 10 of the 11 lattices with both cell sizes the larger cell gives the lower level (median −2.0 kJ/mol).

S14. Sensitivity of the entropy estimate to the threshold

ΔS_{harm} at $\tau = 0.001$, 0.05 and 0.2 eV Å^{-2} (J mol^{-1} K^{-1}) with the fraction of modes used f_{used} at each threshold, for the lattices excluded in S8 and for representative lattices. In all three columns the reference phase enters with its $\tau = 0.05$ average, so the table characterises the sensitivity of the lattice term alone. Over the seven lattices of the applicability set computed at all three thresholds, $|\Delta S(0.001) - \Delta S(0.05)|$ has a median of 0.36 and a maximum of 0.67 J mol^{-1} K^{-1} (bcc Sc; bcc Al 0.54), $|\Delta S(0.2) - \Delta S(0.05)|$ a median of 0.71 and a maximum of 1.63 (Sc), and the change between the extreme thresholds a median of

1.07 and a maximum of 2.30.

Lattice	$\Delta S(0.001)$	f_{used}	$\Delta S(0.05)$	f_{used}	$\Delta S(0.2)$	f_{used}
Al bcc	2.56	0.882	2.03	0.874	0.98	0.852
Ce bcc	31.45	0.153	28.98	0.142	24.96	0.107
Cu bcc	2.44	0.986	2.15	0.982	1.51	0.969
Hf bcc	3.60	0.744	3.35	0.741	2.84	0.732
Ir bcc	9.84	0.669	9.67	0.667	9.31	0.662
Nd bcc	5.21	0.738	4.71	0.731	3.63	0.707
Os bcc	14.83	0.669	14.68	0.667	14.37	0.663
Re bcc	5.71	0.720	5.52	0.718	5.14	0.712
Rh bcc	5.69	0.758	5.53	0.756	5.29	0.753
Ru bcc	13.87	0.684	13.76	0.683	13.52	0.679
Sc bcc	6.47	0.938	5.80	0.927	4.17	0.888
Tc bcc	5.79	0.684	5.52	0.682	5.01	0.674
Th bcc	8.92	0.786	8.56	0.781	7.85	0.766
Ti bcc	4.36	0.779	3.97	0.774	3.25	0.761
W fcc	10.05	0.881	9.79	0.877	9.32	0.869

Table S12: Threshold sensitivity of the harmonic estimate.

Figure S1. Saddle networks of the other five elements

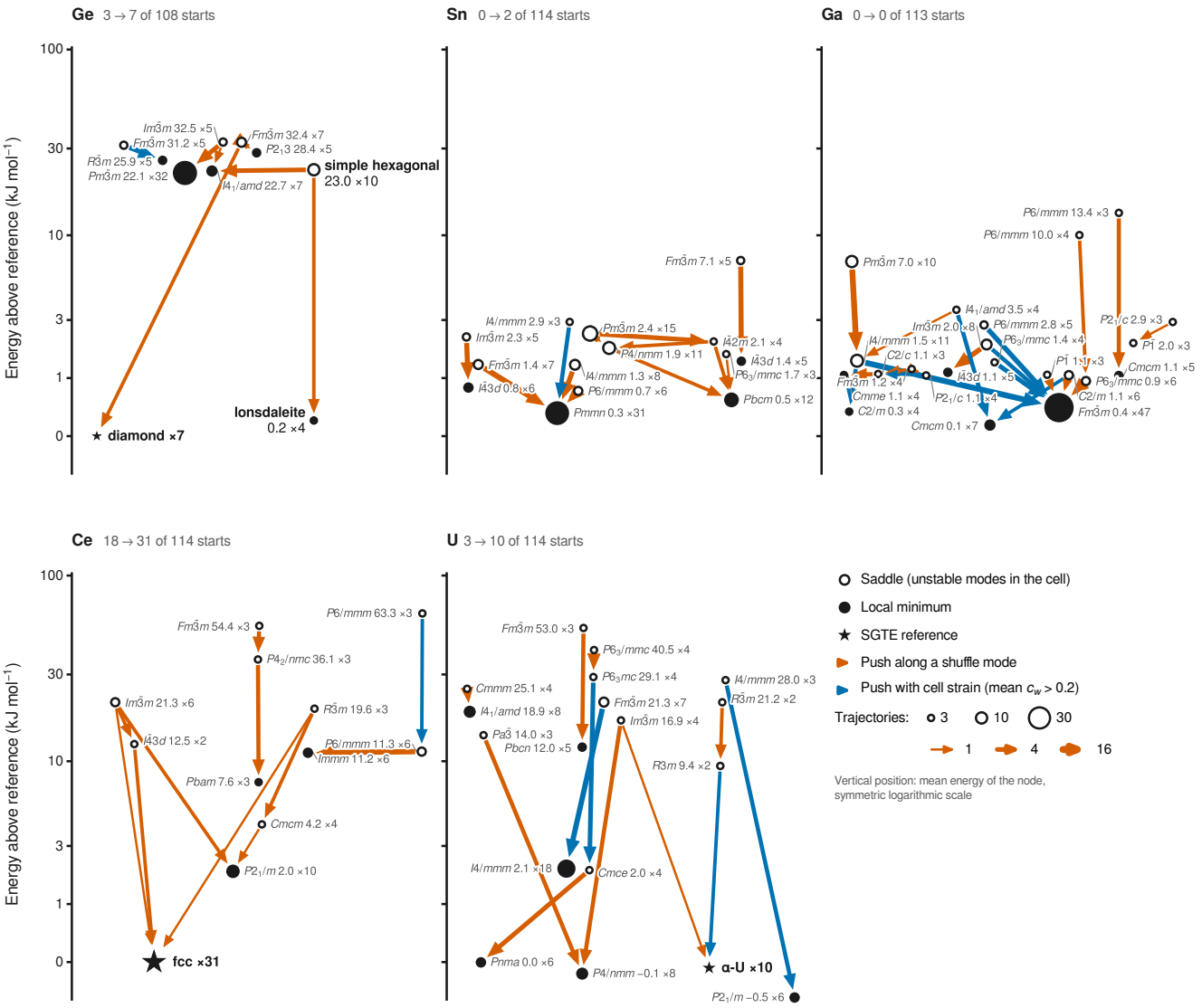

Figure S1: Saddle networks of the blind set for the five elements not shown in Fig. 4 of the main text, drawn as Fig. 4: nodes crossed by at least three trajectories and nodes crossed by two trajectories on paths that reach the reference; vertical position, symbols, colours and the scaling of markers and arrows as in Fig. 4. For Ga and Sn no path through the selected nodes reaches the reference (α-Ga, β-Sn), which is therefore not shown.

S15. Mechanical-relaxation paths

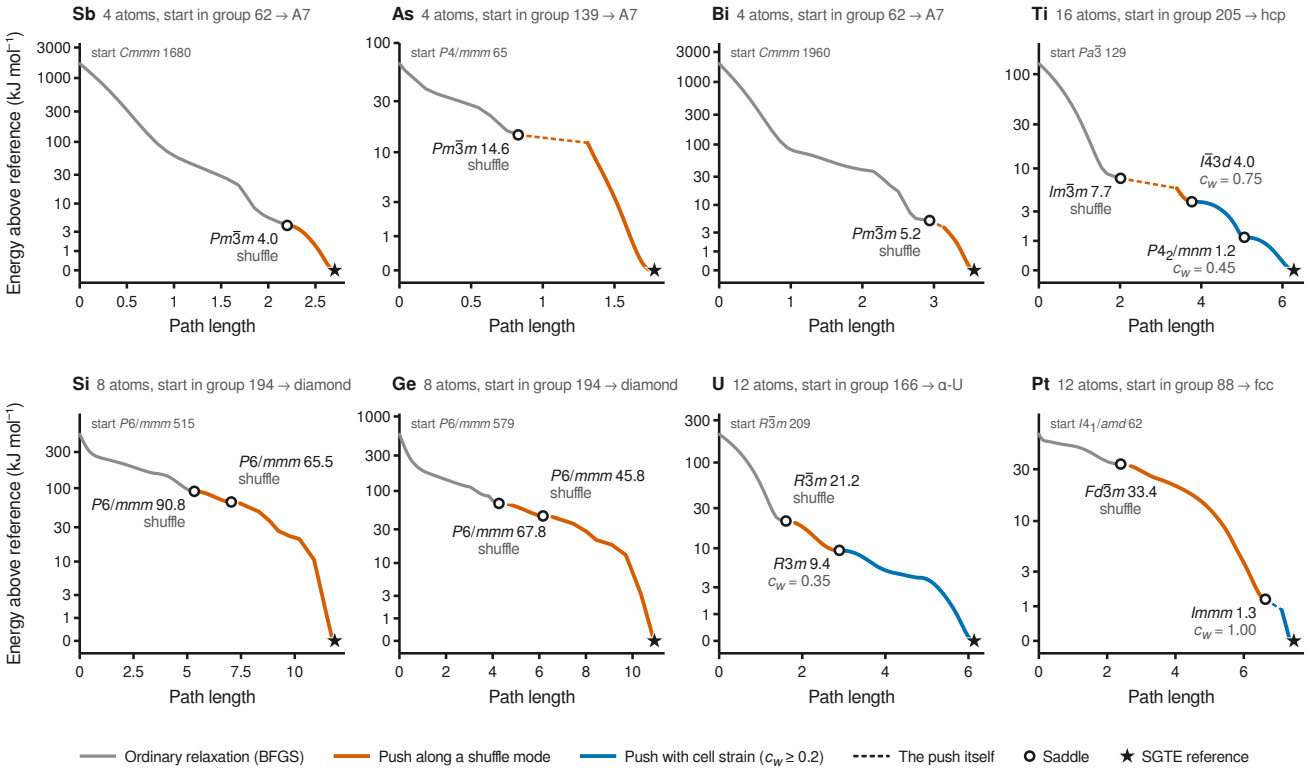

Figure S2: Mechanical-relaxation paths for eight elements (blind set, GRACE-2L-OMAT). Energy above the SGTE reference on a symmetric logarithmic scale against the path length s ($\Delta s^2 = \sum_i |\Delta \mathbf{r}_i|^2 + N\|\Delta\varepsilon\|^2$ between successive frames). Grey: ordinary relaxation, ending at a saddle (open circle). Coloured: the pushes along the softest joint-Hessian mode and the descents that follow them, vermilion for a shuffle and blue for a push with cell strain ($c_w \geq 0.2$); dashed segments are the pushes themselves. Labels give the saddle space group and energy (kJ/mol) and, below, the push from that saddle (shuffle, or its strain fraction c_w). Headers: atoms in the cell, the space group in which the random start was generated and the SGTE reference reached (star); 'start' gives the symmetry and energy of the start.

S16. First descents: strain changes the packing, shuffles change the stacking

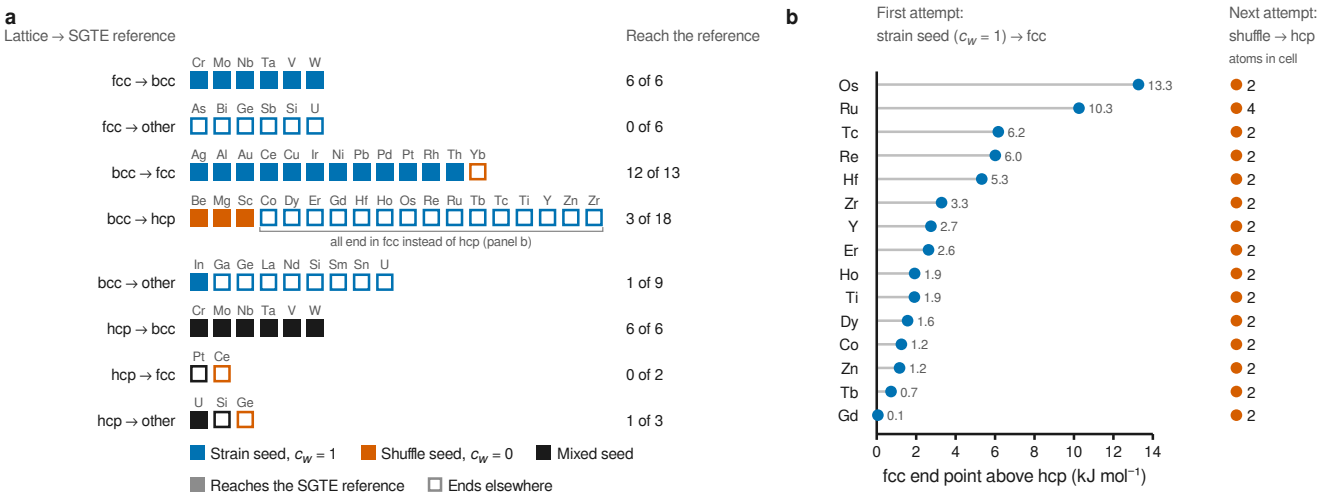

Figure S3: Strain changes the packing, shuffles change the stacking. (a) First descent from 63 mechanically unstable fcc, bcc and hcp element lattices along the softest mode of the smallest cell, grouped by lattice and SGTE reference ("other": a reference that is not fcc, bcc or hcp). Each square is one lattice. Colour: seed type (blue, pure strain $c_w = 1$; vermilion, pure shuffle $c_w = 0$; black, mixed); filled squares reach the reference, open squares end elsewhere. (b) bcc→hcp: a pure strain seed in the one-atom cell ends in fcc (energy above hcp), whereas the next attempt, a pure N-point shuffle in a two-atom cell (Ru: four), reaches hcp, in 15 of 15 cases. For Bi bcc, As hcp, Sb hcp, Ga hcp and Sn hcp the descents were run with an fcc, bcc or hcp structure in place of the SGTE reference (A7, α-Ga, A5); they are excluded from both panels.

S17. Two kinds of lattice instability

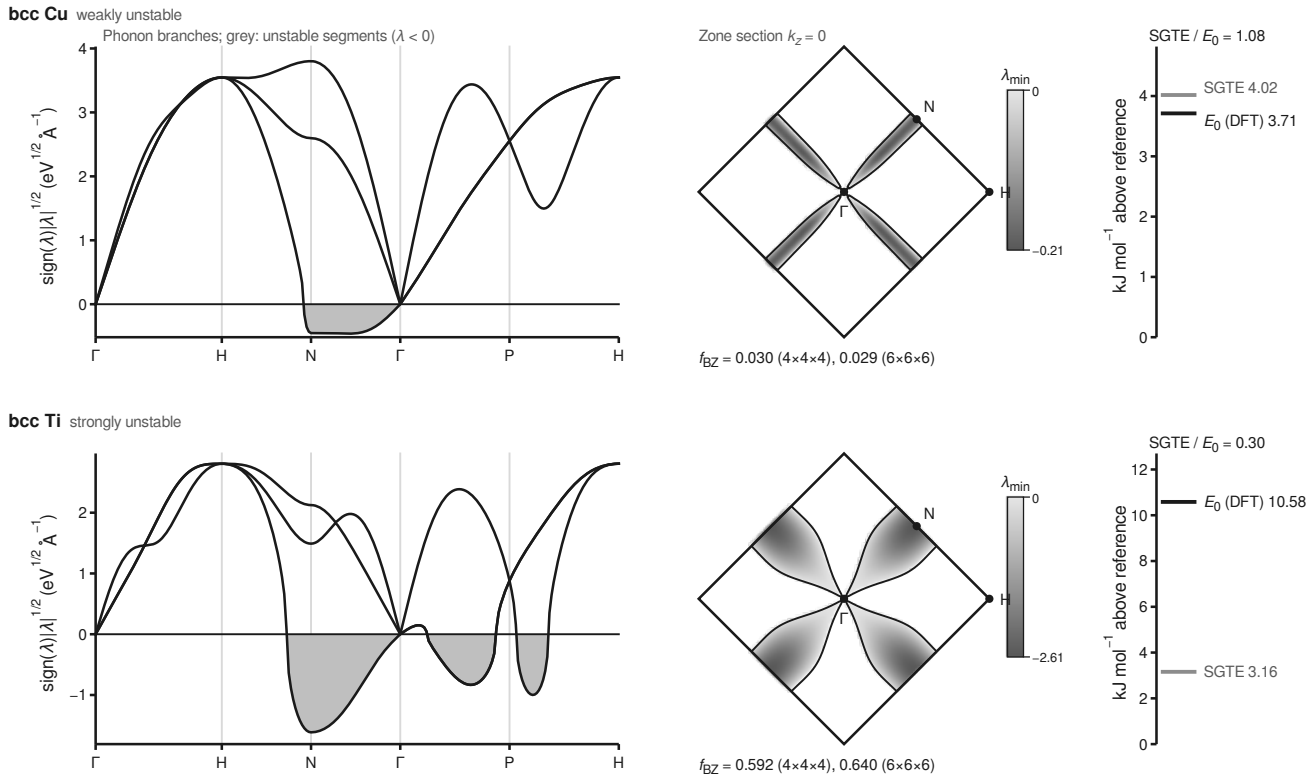

Figure S4: Two kinds of lattice instability. Top: bcc Cu; bottom: bcc Ti. Left: branches $\mathrm{sign}(\lambda)|\lambda|^{1/2}$ of the dynamical matrix along Γ–H–N–Γ–P–H; grey: unstable segments ($\lambda < 0$). Centre: lowest eigenvalue $\lambda_{\min}$ (eV Å^{-2}) on the $k_z = 0$ section of the Brillouin zone, grey where it is negative (darker for a deeper instability), with the $\lambda = 0$ contour; f_{BZ} ($\tau = 0.05$, 20 000 random wave vectors) is given for $4 \times 4 \times 4$ and $6 \times 6 \times 6$ force constants. Right: DFT static energy E_0 (black) and SGTE lattice stability (grey) above the reference. Branches and zone sections are from GRACE-2L-OMAT force constants of a $4 \times 4 \times 4$ supercell of the ideal lattice relaxed with the potential.

S18. Alternative schemes at accounted cost

Scheme	Hits	New hits	Hit rate	Median evaluations per start	Evaluations per hit
ordinary relaxation (BFGS)	47	–	5.0 %	29	830
joint cell–atom Hessian (this work)	173	126	18.6 %	2 036	36 000
atomic modes, fixed cell, same scan	157	110	16.9 %	1 328	34 500
atomic modes, fixed cell, first protocol	141	94	15.1 %	1 705	75 300
strain modes only (TGLE step)	93	46	10.0 %	19	18 000
random push, same amplitudes	230, 231	183, 184	24.7, 24.8 %	18 586	90 300

Table S13: Alternative schemes on the same 931 blind starts ($N = 4$, 8, 12; eleven elements), all starting from the BFGS end point and charged with every evaluation of the potential, including Hessians and candidate scans. "New hits": starts not solved by ordinary relaxation (884). "Same scan": the candidate scan described in the Methods and three descents per push; "first protocol": no scan, six descents per push. Random push: two realisations per start, listed separately.

S19. Energies of saddle hubs and low-lying minima in DFT

Element	Structure	DFT	GRACE
As	simple cubic (hub)	10.4	14.6
Sb	simple cubic (hub)	4.2	4.0
Bi	simple cubic (hub)	4.2	5.2
Si	simple hexagonal (hub)	29.9	30.7
Ge	simple hexagonal (hub)	23.7	23.0
Ti	bct saddle	9.3	6.7
Si	lonsdaleite	+1.1	−0.1
As	$P\bar{3}m1$ minimum	+0.1	−0.4
U	$P2_1/m$ minimum	−0.1	−0.5
U	$P4/nmm$ minimum	+12.5	−0.1

Table S14: Energies above the SGTE reference (kJ/mol) of saddle hubs and of minima that GRACE places below the reference: DFT (PBE, relaxed within the symmetry; Ti bct at the GRACE geometry) versus GRACE-2L-OMAT.